Maximum Efficiency Tracking of a Wireless Power Transfer System With 3-D Coupling Capability Using a Planar Transmitter Coil Configuration

Zhenghao Zhu, Huan Yuan, Cang Liang, Chaoting Wang, Simeng Lv, Aijun Yang, *Senior Member, IEEE*, Jifeng Chu, *Member, IEEE*, Mingzhe Rong, *Senior Member, IEEE*, Xiaohua Wang, *Senior Member, IEEE*, and Aiguo Patrick Hu, *Senior Member, IEEE*

***Abstract*—High degrees of coupling freedom in wireless power transfer (WPT) has emerged as a prominent research topic. The challenge lies in achieving a compact structural design for such systems. This article introduces a planar transmitter configuration composed of three decoupled and separately controlled converters to enable three-dimensional (3-D) WPT to an arbitrarily positioned receiver above the transmitter. By theoretical analysis based on the coupled mode equations, it is found that there is a direct relationship between the dc input voltages and currents of the inverters for achieving the maximum efficiency. The spatial magnetic field is shaped by controlling the input voltages based on the measured currents to achieve the best magnetic field coupling for maximum efficiency tracking, regardless of the positioning and alignment of the power pickup. A practical system is built with a 10 × 10 cm transmitter (with three decoupled coils) and 3.5 × 3.5 cm (single coil) receiver, and it is demonstrated that the system can achieve a power transfer efficiency about 80% within 3 cm above the transmitter under all 3-D coupling conditions.**

***Index Terms*—Magnetic field forming, maximum efficiency, planar coil configuration, wireless power transfer (WPT).**

Manuscript received 16 November 2023; revised 5 March 2024; accepted 20 April 2024. Date of publication 7 May 2024; date of current version 20 June 2024. This work was supported in part by the National Natural Science Foundation of China under Grant U2166214, in part by Shaanxi Natural Science Basic Research Program under Grant 2021JQ-041, in part by the State Key Laboratory of Electrical Insulation and Power Equipment under Grant EIEP21306 and Grant EIPE23314, and in part by the "Sanqin Scholars" Innovation Team Project (Demonstration Innovation Team of Xi'an Jiaotong University for the Key Technology of Advanced DC Power Equipment and Its Industrialization). Recommended for publication by Associate Editor M. Ponce-Silva. (Zhenghao Zhu and Huan yuan contributed equally to this work.) (Corresponding authors: Huan Yuan; Aijun Yang; Xiaohua Wang.)

Zhenghao Zhu, Huan Yuan, Cang Liang, Chaoting Wang, Simeng Lv, Aijun Yang, Jifeng Chu, Mingzhe Rong, and Xiaohua Wang are with the School of Electrical Engineering, Xi'an Jiaotong University, Xi'an 710049, China (e-mail: zzh1997@stu.xjtu.edu.cn; huanyuan@xjtu.edu.cn; liangcang@stu.xjtu.edu.cn; 3122304092@stu.xjtu.edu.cn; lsm087@stu.xjtu.edu.cn; yangaijun@mail.xjtu.edu; jfchu93@xjtu.edu.cn; mzrong@mail.xjtu.edu.cn; xhw@mail.xjtu.edu.cn).

Aiguo Patrick Hu is with the Department of Electrical and Computer Engineering, University of Auckland, Auckland 1142, New Zealand (e-mail: a.hu@auckland.ac.nz).

Color versions of one or more figures in this article are available at https://doi.org/10.1109/TPEL.2024.3397457.

Digital Object Identifier 10.1109/TPEL.2024.3397457

I. Introduction

WIRELESS power transfer (WPT) technology facilitates the provision of power without the necessity of physical connections. This methodology has demonstrated significant convenience and reliability in domains such as consumer electronics, electric vehicles, sensor networks, and various unmanned systems, thus attracting extensive attention from researchers [1], [2], [3], [4], [5], [6], [7]. Commercialization of this technology has been realized in sectors including mobile phones and computers. However, current WPT strategies impose stringent requirements on the positioning of transmitters (Tx) and receivers (Rx), substantially limiting the application of WPT in practical products. The escalating demand for powered devices necessitates enhanced spatial flexibility and system compactness in wireless charging systems.

In order to improve the spatial flexibility of WPT system, some investigations have been conducted. For example, three-dimensional (3-D) Tx coil structure, relay coil and adjustable impedance matching are introduced into WPT [8], [9], [10]. However, a large amount of magnetic leakage leads to the inefficiency of these methods when the position and direction of the Rx change. The magnetic field shaping in the three-dimension space can effectively improve the charging efficiency of the omnidirectional WPT system. Some researchers change the current distribution in the 3-D orthogonal Tx coil array through multiple controlled sources to shape magnetic field [11], [12]. However, 3-D Tx structure has low space utilization and it is difficult to apply in many application scenarios.

Some scholars have done the research of high degree of freedom WPT based on planar coils in recent years. However, relevant research results are relatively few. Kang et al. [13] realized the 3-D magnetic field shaping through a 2-D planar Tx coil array, but the cross coupling between Tx coils is not completely eliminated. Feng et al. [14] proposed a fully decoupled coil array to realize 3-D rotating magnetic field. The above work achieves magnetic field shaping by phase shifting. However, phase shifting will increase magnetic field leakage and reduce efficiency [15]. Furthermore, each of these approaches necessitates the acquisition of the receiving coil's positional and directional information, a process that not only substantially

heightens system complexity but also fails to maintain universality across various devices. And these above methods all require more than four Tx coils.

This article introduces a WPT system with high degrees of coupling freedom based on a planar coil configuration, which can provide power to receivers of any position and orientation. The transmitter of this system consists of only three coils, and a 3-D magnetic field is shaped by a compact planar coil structure. The Tx coils are decoupled. Maximum efficiency tracking can be achieved by changing the input voltages based on the measured currents of inverters. The main research content and innovations of this article can be summarized as follows.

1) A generic decoupling and design method for a planar transmitter used for 3-D magnetic field forming is provided. The mechanism of achieving a 3-D magnetic field shaping with this scheme is clarified. This greatly reduces the installation space for wireless power transfer system with 3D coupling capability.
2) Established a multitransmitter coil WPT system circuit model using *LCC*-S topology based on the coupling mode model, and found the direct relationship between the dc input voltages and currents of the inverters for achieving the maximum efficiency.
3) A scheme of changing the input voltages based on the measured currents in the inverters is proposed to obtain the optimal magnetic field and tracking the maximum system efficiency. Compared with previous research, the wireless communication module is eliminated.

The rest of the article is organized as follows. Section II introduces the design scheme of the planar coil group and supplemented by an illustrative example. Section III builds the proposed system's circuit model and Section IV introduces the method of maximum efficiency tracking. Section V covers the experimental setup and its validation. Finally, Section VI concludes the article.

II. Transmitter Configuration and Magnetic Field Analysis

A. Design Principles of the Planar Transmitter

The system in discussion features a planar transmitter designed to generate a controllable magnetic field in space. For optimal power transfer efficiency, the planar transmitter should maintain maximum mutual inductance with an Rx coil placed arbitrarily in space. A schematic demonstration of the coupling mechanism with a single Tx coil and an Rx coil is shown in Fig. 1(a).

In scenarios with a diminutive Rx coil, for simplicity, the magnetic induction intensity of the point *P* (the center of an Rx coil) is chosen to deduce the mutual inductance. According to Biot Savart's law [16], the magnetic induction intensity produced by the Tx coil at the point *P* is denoted as $\vec{B}_P$, which is

$$\vec{B}_p = \frac{\mu_0 I}{4\pi} \int \frac{d\vec{L} \times \vec{r}}{r^3} \tag{1}$$

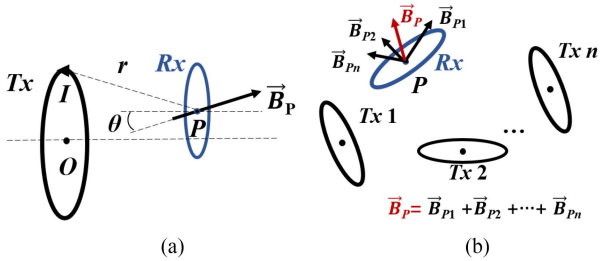

Fig. 1. Magnetic field at Rx coil generated by (a) a single Tx coil and (b) multiple Tx coils.

where μ_0 is the vacuum permeability, I denotes the excitation current, $\vec{L}$ is the length vector of the current element, $\vec{r}$ symbolizes the distance vector from the corresponding current element to the point *P*, and θ represents the angle between $\vec{r}$ and the orthogonal vector of the Rx coil's plane. Based on the definition of the mutual inductance, the mutual inductance *M* between the Tx coil and the Rx coil is defined as

$$M = \sum d\Phi / I \doteq B_{\mathrm{P}} S \cos\theta. \tag{2}$$

Thus, for a fixed magnetic induction intensity $\vec{B}_P$ at point *P*, the angle between the direction of $\vec{B}_P$ and the Rx coil plane determines the mutual inductance. Assuming that there are multiple Tx coils, the direction of the magnetic field generated by the Tx coil *i* is $\vec{e}_i$. Coupling mechanism with multiple Tx coils and an Rx coil is shown in Fig. 1(b), and the magnetic induction at point *P* can be expressed as

$$\vec{B}_P = \sum \vec{B}_{Pi} = \sum \frac{4N_i\mu_0}{\sqrt{2}l} I_i \vec{e}_i. \tag{3}$$

According to (3), using *n* Tx coils will produce a total magnetic field $\vec{B}_P$ at point *P* that is the vector sum of the magnetic fields generated by each Tx coil at *P*. When $n \geq 3$, if $\vec{B}_{P1}$, $\vec{B}_{P2}$, and $\vec{B}_{P3}$ are linearly independent, $\vec{B}_P$ can point to any spatial direction. Under these conditions, for any arbitrarily placed Rx coil, the excitation currents can be adjusted to make the angle θ between $\vec{B}_P$ and the normal vector of Rx be zero, thereby ensuring maximum mutual inductance between the transmitter and receiver.

Introducing multiple adjacent Tx coils could lead to cross-coupling among them. This scenario suggests that each Tx coil could potentially act as an Rx coil for the others, a situation that may cause variations in the reflected impedance of each Tx due to changes in the excitation current. Such variations might deviate the system's magnetic field from its intended configuration, adversely affecting the transfer efficiency. Therefore, addressing cross-coupling among Tx coils becomes critical for maintaining system efficacy.

Drawing from this analysis, to achieve magnetic field shaping through excitation current control, ensuring the highest mutual inductance between Tx and Rx coils, the Tx coil group's design should satisfy the following two conditions.

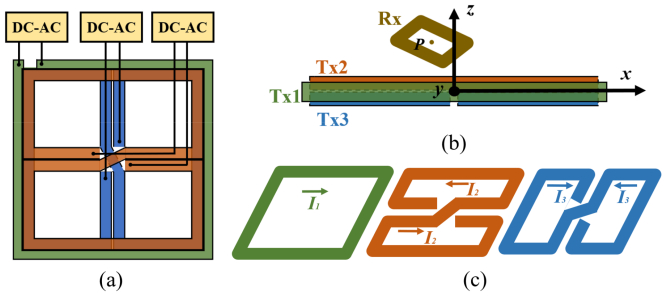

Fig. 2. Tx coil group design. (a) Top view. (b) Front view. (c) Independent structure.

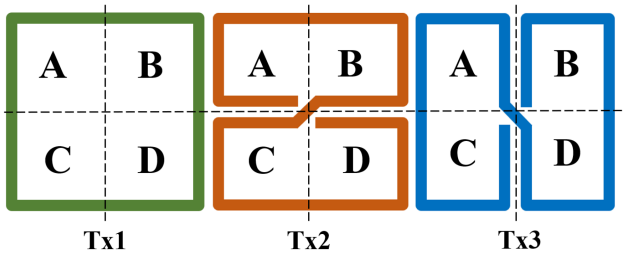

Fig. 3. Intricate depiction of the Tx coils.

1) Employ at least three Tx coils. There is no mutual coupling among these Tx coils.
2) Ensure each Tx coil's magnetic induction vector at the Rx coil remains linearly independent.

B. Magnetic Field Analysis of a Planar Transmitter

Building upon the design principles elucidated in the preceding section, a planar Tx assembly has been proposed for a WPT system with enhanced spatial freedom. This configuration features three separate Tx coils as shown in Fig. 2. Tx1 and Tx2 are double-D (DD) coils, arranged to overlap each other. In pursuit of the thinnest possible design for the transmitter, the square coil, Tx3, is slightly larger than both Tx1 and Tx2 and encases them. To better meet the needs of omnidirectional wireless charging for mobile devices, a relatively smaller square coil has been adopted as the Rx coil. The excitation currents within the three Tx coils are denoted as I_1, I_2, and I_3, respectively.

Initially, minimizing mutual inductance between the Tx coils is crucial to avoid potential interference in their transmission impedances. To aid in calculating this inductance, Fig. 3 provides an intricate depiction of the Tx coils coupled with a comprehensive spatial region segmentation.

According to the formula of mutual inductance between two coils, the mutual inductances between Tx coils are

$$\begin{cases} M_{12} = \left(\Phi_{\mathrm{A}21} + \Phi_{\mathrm{B}21} + \Phi_{\mathrm{C}21} + \Phi_{\mathrm{D}21}\right)/I_1 = 0 \\ M_{13} = \left(\Phi_{\mathrm{A}31} + \Phi_{\mathrm{B}31} + \Phi_{\mathrm{C}31} + \Phi_{\mathrm{D}31}\right)/I_1 = 0 \\ M_{23} = \left(\Phi_{\mathrm{A}32} + \Phi_{\mathrm{B}32} + \Phi_{\mathrm{C}32} + \Phi_{\mathrm{D}32}\right)/I_2 = 0. \end{cases} \tag{4}$$

In the above-mentioned equation, $\Phi_{\mathrm{A}\,ij}$ represents the magnetic flux generated by the current in Tx j that passes through area A of the Tx i coil. Taking into account the symmetry of these three coil structures, in this tricoil transmitter configuration, there is an absence of cross-coupling amongst the paired Tx coils, aligning with the design prerequisites highlighted previously. In real applications, given potential minor structural deformations, unforeseen mutual inductance might arise between the Tx coils, complicating the process of impedance matching.

Ensuring the linear independence of magnetic induction intensities generated by the trio of transmission coils at the Rx position is crucial. For streamlined analysis, initial calculations focused on magnetic induction intensities proximate to the Z-axis. The outcomes for the three coils on the Z-axis are

$$\begin{aligned} B_{X1} &= 0 \\ B_{Y1} &= 0 \\ B_{Z1} &= \frac{\mu_0 I l}{8\pi\left[(l/2)^2 + h^2\right]^{\frac{3}{2}}} \\ B_{X2} &= 0 \\ B_{Y2} &= \frac{\mu_0 I h}{4\pi\left[(l/2)^2 + h^2\right]^{\frac{3}{2}}} \\ B_{Z2} &= 0 \\ B_{X3} &= 0 \\ B_{Y3} &= \frac{\mu_0 I h}{4\pi\left[(l/2)^2 + h^2\right]^{\frac{3}{2}}} \\ B_{Z3} &= 0 \end{aligned} \tag{5}$$

where h represents the height from the point to be measured to the Tx plane, l is the side length of Tx, and B_{Xi} denotes the component of the magnetic induction strength generated by Tx i in the X-axis direction. As discerned from (5), proximate to the Z-axis, Tx1, Tx2, and Tx3 induce magnetic fields along the Z, X, and Y axes, respectively. Induction intensities along alternate directions appear minimal. This signifies the orthogonal nature of their magnetic induction intensities around the Z-axis.

Utilizing finite-element simulations provides a comprehensive view of the spatial dispersion patterns inherent to the magnetic induction intensities produced by the three-coil structure. Fig. 4 visually conveys the spatial magnetism triggered by the coils under electrical stimulation.

Primarily, in the areas directly above the coils, the magnetic fields generated can be interpreted as orthogonal to each other. However, as one approaches the edges of the coil, there's a noticeable decrease in the spatial angle of magnetic induction intensity generated by Tx coils. This suggests that the complexity of magnetic field synthesis increases when the Rx moves closer to the transmitter's boundaries. Given that the Rx covers a specific surface area, the magnetic flux lines passing through it do not follow a uniform direction. The combined magnetic induction effects from the three transmission coils acting on the Rx are considered to be linearly independent. As a result, this arrangement has the capability to generate a 3-D magnetic field in any desired direction above the Tx. To further illustrate,

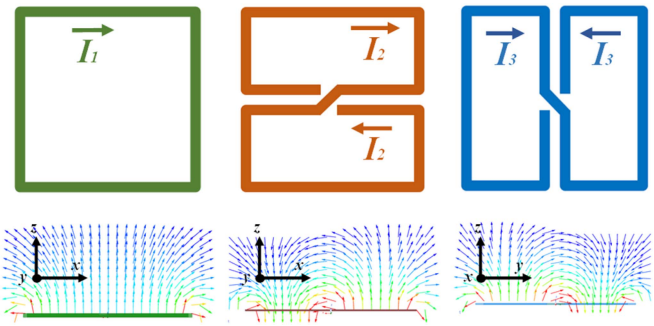

Fig. 4. Magnetic field of three Tx coils.

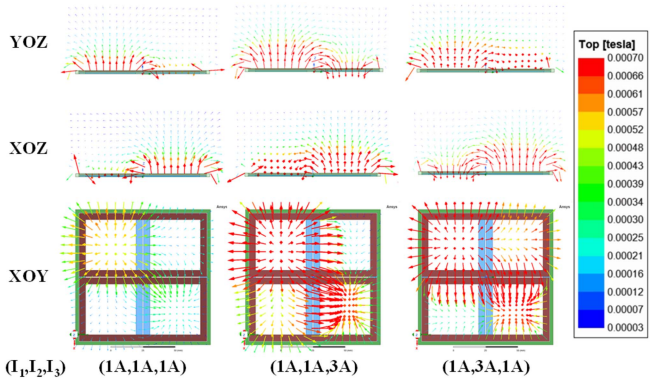

Fig. 5. Magnetic field distribution under different current excitations.

TABLE I
SIMULATION RESULTS FOR THE SELF-INDUCTANCE AND MUTUAL INDUCTANCE OF THE COILS

	Tx1	Tx2	Tx3
Tx1	62.9 μH	0.25 nH	0.53 nH
Tx2	0.25 nH	77.6 μH	0.15 nH
Tx3	0.15 nH	0.3 μH	77.7 μH

Fig. 5 shows magnetic field distribution under different current excitations.

It can be observed that the direction and magnitude of the magnetic field at a fixed position change with variations in current. Therefore, by altering the amplitude of the current, the magnetic field at the location of the Rx coil can be enhanced, reducing magnetic leakage in other directions, thereby improving the overall efficiency of the system. The simulation results for the self-inductance and mutual inductance of the three transmitting coils are shown in Table I.

It can be seen that the mutual inductance between the coils of this structure is almost zero, indicating that they are decoupled, which matches the theoretical results.

C. Extended Discussion

The scheme proposed is applicable not only to the configuration comprising two DD coils and a Q coil but also extends to other coil arrangements that satisfy the conditions outlined in Section II-A.

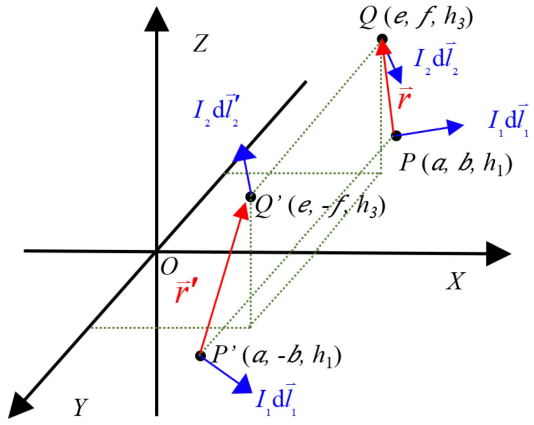

Fig. 6. Positional relationships between current elements.

Indeed, when the configuration of three coils, symmetric along both the X and Y axes, satisfies the following conditions: Current distribution in Tx1 is symmetric along the X-axis and antisymmetric along the Y-axis; current distribution in Tx2 is symmetric along the Y-axis and antisymmetric along the X-axis; and current distribution in Tx3 is antisymmetric along both the X and Y axes, then the three coils can be mutually decoupled. This arrangement ensures that the magnetic fields generated by each coil do not interfere with each other, allowing for independent operation and control of each coil within the system. Considering three coils configured as previously described, the mutual inductance M between coils can be calculated by integrating the magnetic flux Φ generated by current elements at each point within a coil [1]. Taking Tx1 as an example, assume a current element at point P (a, b, h_1) on Tx1 is $I_1 \mathrm{d}l_1$, with its vector direction being (c, d, h_2). Then, for a symmetric point P′ along the x-axis $(a, -b, h_1)$, the current element is $I_1 \mathrm{d}l_1'$, and its vector direction is $(c, -d, h_2)$. Similarly, for a point Q (e, f, h_3) on Tx2 or Tx3, there is a current element $I_2 \mathrm{d}l_2$, with its vector direction being (g, h, h_4). And for a symmetric point Q′ along the x-axis $(e, -f, h_3)$, the current element is $I_2 \mathrm{d}l_2'$, with its vector direction being $(-g, h, -h_4)$. The positional and directional relationships between these current elements are illustrated in Fig. 6.

The magnetic flux $\mathrm{d}\Phi$ generated by the current element $I_1 \mathrm{d}l_1$ on the area element enclosed with $I_2 \mathrm{d}l_2$ can be expressed as

$$\mathrm{d}\Phi = \mathrm{d}\vec{B} \cdot \mathrm{d}\vec{S} = \mathrm{d}\vec{B} \cdot \left(\mathrm{d}\vec{l}_2 \times \vec{r}\right) = \frac{4\pi I}{\mu_0 r^3} \left(\mathrm{d}\vec{l}_1 \times \vec{r}\right) \cdot \left(\mathrm{d}\vec{l}_2 \times \vec{r}\right). \tag{6}$$

Corresponding to this, the magnetic flux $\mathrm{d}\Phi'$ generated by the current element $I_1 \mathrm{d}l_1'$ on the area element enclosed with $I_2 \mathrm{d}l_2'$ can be expressed as

$$\mathrm{d}\Phi' = \mathrm{d}\vec{B}' \cdot \mathrm{d}\vec{S} = \mathrm{d}\vec{B}' \cdot \left(\mathrm{d}\vec{l}_2{}' \times \vec{r}\right) = \frac{4\pi I}{\mu_0 r^3} \left(\mathrm{d}\vec{l}_1{}' \times \vec{r}\right) \cdot \left(\mathrm{d}\vec{l}_2{}' \times \vec{r}\right). \tag{7}$$

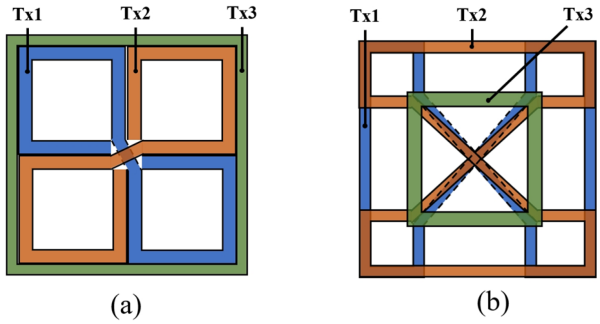

Fig. 7. Two alternative coil configurations.

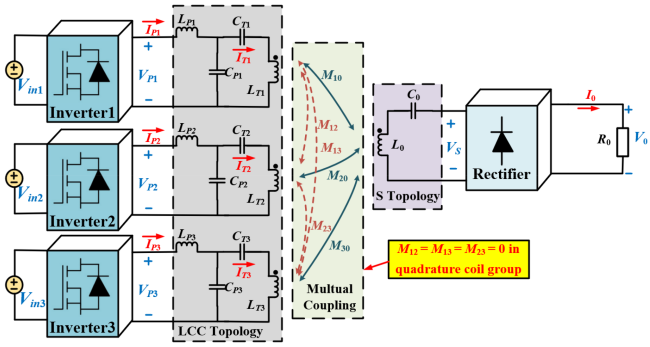

Fig. 8. System circuit topology.

After substituting coordinates into the expression for magnetic flux, it can be derived that

$$\mathrm{d}\Phi' = -\mathrm{d}\Phi. \tag{8}$$

This means the total magnetic flux generated by Tx1 within Tx2 (Tx3) can be obtained by combining the magnetic flux generated by the parts of Tx1 above and below the X-axis within Tx2 (Tx3) which expressed as

$$\Phi_{Total} = \iint_{Tx1,Tx2} \Phi = \iint_{\substack{Tx1aboveX\\Tx2aboveX}} \Phi + \iint_{\substack{Tx1aboveX\\Tx2belowX}} \Phi + \iint_{\substack{Tx1belowX\\Tx2aboveX}} \Phi + \iint_{\substack{Tx1aboveX\\Tx2blowX}} \Phi = \iint_{Tx1aboveX,Tx2} \Phi + \iint_{Tx1aboveX,Tx2} \Phi' = 0. \tag{9}$$

The magnetic flux generated by Tx1 within Tx2 and Tx3 is zero, indicating that the two coils are completely decoupled. Similarly, it can be concluded that Tx1, Tx2, and Tx3 are mutually decoupled from each other. Based on this conclusion, any coil configuration that meets actual usage requirements can be designed. Fig. 6 illustrates two alternative coil configurations that are compatible with the proposed approach.

Fig. 7(a) and (b) expands upon the dual DD coil and square coil structure. These indicate the high degree of adaptability of the proposed solution.

This adaptability underscores the versatility of the proposed approach, making it applicable to a wide range of coil configurations beyond the initially described tricoil structure. Such flexibility facilitates the design of WPT systems that can cater to diverse operational requirements and spatial constraints, significantly broadening the scope of potential applications.

III. Proposed System and Modeling

For WPT systems with high spatial degrees of freedom, the complex positioning of the receiver implies significant magnetic leakage and low efficiency. Adjusting the spatial magnetic field can minimize this system leakage. Typically, magnetic field shaping requires position information of the receiver, but this method demands an intricate communication link and is not universally applicable to different transmitter structures. In fact, the flux variation between the Tx and Rx coils can be mapped to the system's mutual inductance parameters, reflecting the effectiveness of magnetic field shaping through system efficiency. It is crucial to explore a method to easily reshape the magnetic field based on circuit parameters and enhance system efficiency. This section establishes the system's circuit model mathematically and analyzes the relationship between system efficiency and primary-side parameters.

TABLE II
Symbolic Representation of Electronic Components

Symbol	Quantity
I_{T1}, I_{T2}, I_{T3}, I_0	Current amplitudes of Tx coil 1, 2, 3, and Rx coil
I_{P1}, I_{P2}, I_{P3},	Output currents of inverters
V_{in1}, V_{in2}, V_{in3}, V_0	Voltage amplitudes of Tx 1, 2, 3 and Rx
V_{P1}, V_{P2}, V_{P3}	Output voltages of inverters
L_1, L_2, L_3, L_0	Self-inductances of Tx coil 1, 2, 3, and Rx coil
R_1, R_2, R_3	Coil resistances of Tx coil 1, 2, 3
R_L, R_0	Coil and load resistances of Rx coil
C_1, C_2, C_3, C_0	Resonant capacitances of Tx coil 1, 2, 3, and Rx coil
M_{n0}	Mutual inductances between Tx coil n and Rx coil

The previous section mentioned that a constant Tx coil current is required to maintain the stability of the magnetic field shaping effect under varying coupling conditions. This article selects the *LCC*-S topology. With this topology, the Tx current remains constant even under load fluctuations. The system topology, as shown in Fig. 8, consists of three Tx coils and one Rx. The symbolic representation of electronic components is shown in Table II . The Tx coils include a full-bridge inverter, resonant coil, and compensating capacitor, whereas the Rx comprises the Rx coil, compensating capacitor, rectifying circuit, and load.

Generally, for a system with a single Tx coil and Rx coil, the magnitude of the induced current relates to the coupling coefficient K, where K is a positive scalar and always maintains a positive value in mathematical expressions. However, when the number of Tx coils exceeds two, the direction of the current generated by multiple Tx coils through magnetic coupling resonance in the same Rx coil may differ. This article defines the coupling coefficient K as a scalar that can take negative values for convenience in calculations. When the direction of the input current corresponds to Fig. 2, K_1 is defined as positive. When the induced current in the Rx coil from Tx2 is in the same direction as that produced by Tx1, K_2 is positive; otherwise, it is negative.

The same applies to K_3. It is important to note that this definition is solely based on coil positioning and is not related to current amplitude and phase. The advantage of this definition is that high degree of freedom WPT system modeling requires only a unified equation, eliminating the need for different equations when the Rx coil is in various positions.

The coupled mode theory (CMT) is used to analyze the relationships between the strongly coupled system [17], [18]. To describe WPT schemes with Txs and Rx, we proposed a model based on coupled-mode theory of a higher order resonant system whose dynamics equations are described as

$$\begin{aligned}\frac{\mathrm{d}a_i}{\mathrm{d}t} &= -(\Gamma_i - j\omega_i)a_i + jk_{i0}a_0 + S_+ \\ \frac{\mathrm{d}a_0}{\mathrm{d}t} &= -(\Gamma_0 + \Gamma_{L0} - j\omega_0)a_0 + \sum_{i=1}^{3} jk_i a_0 \end{aligned} \tag{10}$$

where a_i and a_0 represent the time domain field amplitudes of Tx i and Rx, respectively, such that $|a_{i,0}|^2$ represent the energies stored in corresponding resonator; ω_i and ω_0 are the working frequency of Tx i and Rx; k_i is the coupling rate between the Tx coil i and the Rx coil, which depends on frequency and coupling coefficient K. Γ_0 and Γ_i are the decay rate due to absorption and radiated loss in Rx i and Tx i; Γ_L is the decay rate due to a load resistor in Rx; and S_+ is external excitation to the resonator, which appears only in Txs.

IV. Maximum Efficiency Tracking

The time domain field amplitudes of the three Tx coils can be expressed in complex form as

$$a_i = A_i e^{j(\omega t + \varphi_i)} \tag{11}$$

where A_i is the amplitude of time domain mode signal of Tx i, which is a variable related to the energy of the resonator and proportional to the amplitude of the current in the coil.

In addition, the decay rate and the coupling rate have the following relationships with the circuit parameters:

$$\Gamma_i = \frac{R_i}{2L_i}, \quad \Gamma_L = \frac{R_L}{2L_0}, \quad \Gamma_0 = \frac{R_0}{2L_0}, \quad k_i = \frac{\omega_0 K_i}{2}. \tag{12}$$

The power dissipated at Tx i, Rx, and load R_i are denoted as P_i, P_0, and P_L, respectively, and they can be expressed as

$$\begin{aligned} P_i &= 2\Gamma_i |A_i|^2 \\ P_0 &= 2\Gamma_0 |A_0|^2 \\ P_L &= 2\Gamma_L |A_L|^2. \end{aligned} \tag{13}$$

Through the formula (13), it can be calculated that the overall efficiency of the system is

$$\begin{aligned}\eta_0 &= \frac{P_0}{\sum_{i=1}^{3} P_i + (P_0 + P_L)} \\ &= \frac{\left[\Gamma_0 |A_0|^2\right] / \sum_{i=1}^{3} \left(\Gamma_i |A_i|^2\right)}{1 + \left[\left(\Gamma_0 + \Gamma_L\right)|A_0|^2\right] / \left[\sum_{i=1}^{3} \left(\Gamma_i |A_i|^2\right)\right]}. \end{aligned} \tag{14}$$

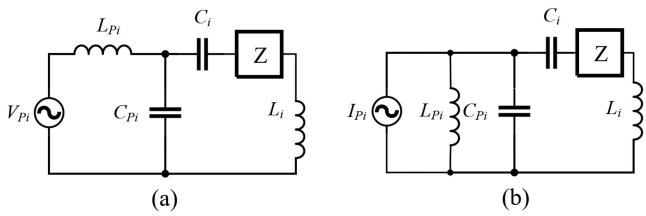

Fig. 9. *LCC* primary side topology. (a) System with a voltage input. (b) Its Thevenin equivalent.

When Tx and Rx work at resonance frequency at the same time, the amplitude of time domain mode signal can be expressed as

$$|A_0| = \frac{\left|k_1 A_1 e^{j\varphi_1} + k_2 A_2 e^{j\varphi_2} + k_3 A_3 e^{j\varphi_3}\right|}{(\Gamma_0 + \Gamma_L)}. \tag{15}$$

This shows that efficiency of the system is a function of the current phase of the Tx coils, and the equivalent coupling rate k_0 between all Rxs and Tx i is defined as

$$k_0 = \frac{\left|k_1 A_1 e^{j\varphi_1} + k_2 A_2 e^{j\varphi_2} + k_3 A_3 e^{j\varphi_3}\right|}{\sqrt{\sum_{i=1}^{3} \left(\Gamma_i |A_i|^2\right)}}. \tag{16}$$

Efficiency increases monotonically with k_0. Leveraging Cauchy–Schwarz inequality, an inequality conforming to formula (16) is established, expressed as

$$k_0 \le \frac{k_1 A_1 + k_2 A_2 + k_3 A_3}{\sqrt{\sum_{i=1}^{3} \left(\Gamma_i |A_i|^2\right)}} \le \sqrt{\sum_{i=1}^{3} \left(\frac{k_i}{\sqrt{\Gamma_i}}\right)^2}. \tag{17}$$

Therefore, according to the conditions of the equation, efficiency of this WPT system can be maximized when the phases of three input currents are in-phase or reverse phase. This is because when there is a phase difference in the currents of the three Tx coils, the composite magnetic vector direction at the Rx is not fixed but rather a rotating vector. The magnetic vector in the direction of the Rx coil's normal vector is responsible for inducing current in the coil, whereas components in other directions act as magnetic leakage, subsequently reducing the system's efficiency.

Under the equality condition of the Cauchy–Schwarz inequality, the amplitudes of the currents in Tx coils are

$$I_1 : I_2 : I_3 = \frac{k_1\sqrt{L_1}}{R_1} : \frac{k_2\sqrt{L_2}}{R_2} : \frac{k_3\sqrt{L_3}}{R_3}. \tag{18}$$

Since there is no mutual inductance between the Tx coil and Rx coil, each Tx can be analyzed independently. The primary side topology of the *LCC* and its Thevenin equivalent are illustrated in Fig. 9 [19], [20].

With L_{Pi} and C_{Pi} in resonance, the primary side topology of the *LCC* effectively acts as a constant current source for the Tx coils, and the current can be described as

$$I_{Ti} = \frac{V_{Pi}}{\omega L_{Pi}}. \tag{19}$$

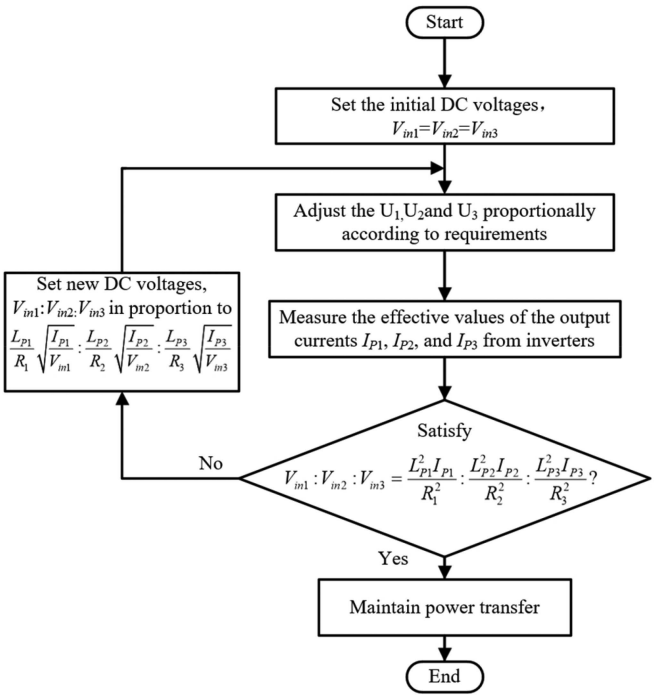

Fig. 10. Flowchart of power transfer process.

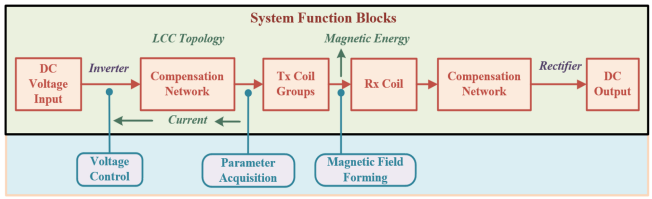

Fig. 11. System function block.

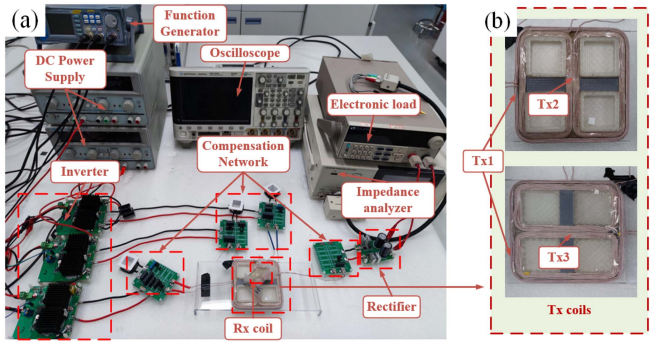

Fig. 12. Experimental setup. (a) Overall platform. (b) Coil details.

In the absence of considering the internal resistance of coils, the effective value of the current I_{Pi} in the compensation circuit can be represented as

$$I_{Pi}=\frac{P_i}{V_{Pi}}=\frac{V_{Pi}M_i^2}{L_{Pi}^2R_L}. \tag{20}$$

In the WPT system featuring an *LCC*-S topology, the output voltages V_{Pi} of inverters are

$$V_{Pi}=\frac{2\sqrt{2}V_{ini}}{\pi}. \tag{21}$$

When the load changes, the conditions of expected input voltage $V+$ *ini* for maximum efficiency can be deduced as

$$V_{in1}^+:V_{in2}^+:V_{in3}^+=\frac{L_{P1}}{R_1}\sqrt{\frac{I_{P1}}{V_{in1}}}:\frac{L_{P2}}{R_2}\sqrt{\frac{I_{P2}}{V_{in2}}}:\frac{L_{P3}}{R_3}\sqrt{\frac{I_{P3}}{V_{in3}}}. \tag{22}$$

By detecting the current value of I_{Pi} and input voltage V_{ini}, the relation of expected input voltage $V+$ *ini* can be calculated. Then, adjust the input voltage according to the formula (22), the system can work with the highest efficiency real-time. Fig. 10 illustrates the flowchart detailing this power transfer process.

On this basis, a model of high spatial freedom WPT system with receiver is proposed. The functional block diagram and energy flowchart are shown in Fig. 11.

The system channels electrical energy from three inputs into magnetic energy via the Tx coil, showcasing its capability for magnetic field shaping, which is evident in its ac–ac transfer efficiency. Upon the Rx coil's integration into the system, it detects variations in the currents IP, enabling the adjustment of the dc input voltage in line with (16). Through the modification of the input voltage using the *LCC*-S topology, the input current to the Tx coil is regulated, facilitating the achievement of optimal magnetic field configuration and the pursuit of maximal efficiency tracking. Subsequently, the ac/dc converter converts the induced electromotive force into a steady dc power output, culminating the wireless power transmission cycle.

V. Experimental Study

A. Experiment Setup

A WPT system prototype with triple planar Tx coils and a Rx was built to validate the proposed model and results. Fig. 12 presents a schematic of the experimental setup. A direct current source links to three full-bridge inverters, which in turn supply the system with alternating current. The system employs a full-bridge rectification circuit to convert the ac voltage into dc voltage. A signal generator manages the system's phase and frequency. The coupling assembly incorporates three Tx coils and a singular Rx coil. The assembly of Tx coils features a square layout, with both Tx2 and Tx3 characterized as DD coils, each spanning 10 cm with 15 windings. Meanwhile, Tx1, a square coil, envelops the exterior with 10 windings. The Rx coil is square-shaped, sizing up at 3.5 cm $\times$ 3.5 cm with 20 windings. For a detailed view of these coils, refer to Fig. 12(b).

An operating frequency of 500 kHz has been selected. The system utilizes an *LCC*-S compensation network, constituted by inductors crafted with Litz wire and an ensemble of capacitors. On the receiving end, the circuitry features a full-bridge rectifier designed using uncontrolled diodes. The actual parameters for the high degree of freedom WPT system are delineated in Table III.

Upon carrying out measurements across the three sets of Tx coils, a minor degree of mutual inductance was detected among them. This observed mutual inductance could primarily result from inconsistencies in manual winding processes and

TABLE III
ACTUAL PARAMETERS OF THE WPT SYSTEM

Symbol	Value	Symbol	Value	Symbol	Value
L_{P1}	5.1 μH	L_2	63.2 μH	R_3	1.2 Ω
L_{P2}	5.0 μH	L_3	64.6 μH	R_L	20 Ω
L_{P3}	5.0 μH	R_1	1.3 Ω	R_0	0.8 Ω
L_1	71.2 μH	R_2	1.1 Ω	L_0	72.6 μH

TABLE IV
MUTUAL INDUCTANCES ACROSS TX COILS

	Tx1	Tx2	Tx3
Tx1	/	0.6 μH	0.4 μH
Tx2	0.6 μH	/	0.3 μH
Tx3	0.4 μH	0.3 μH	/

minor deformations occurring after winding. Table IV details the mutual inductance values identified among these Tx coils, which are markedly lower than the mutual inductance measured between the Tx and Rx coils. The minor mutual inductances observed are unlikely to significantly influence the transmission process, leading to the deduction that the three Tx coils are effectively decoupled.

B. Maximum Efficiency

To validate the conditions stipulated for optimal efficiency from the prior section, we executed a fixed-position energy transfer experiment. The Rx coil was inclined with its normal vector defined as (1,1,1), aligning with the coordinate system illustrated in Fig. 2. The distance from the center of the Rx coil to Tx was 2 cm. And a 20 Ω resistor is utilized as the load. Variations in the currents and phases of Tx coils yielded the waveform, depicted in Fig. 13. Within each representation, from the top down, the waveforms denote the induced voltage in the Rx coil, followed by currents in Tx1, Tx2, and Tx3, respectively.

From Fig. 13(a), with all Tx currents at 0.33 A, the induced voltage measures around 12 V, and the system's efficiency is 74.7%. In Fig. 13(b), maintaining the Tx current amplitudes at 0.33 A and altering the phases to 0, $\pi/6$, and $\pi/3$, respectively. The Rx's induced voltage drops to approximately 6 V, the system's efficiency decreases to 52.1%. This decrement stems from increased magnetic leakage due to the rotating magnetic field, aligning with the previously discussed phase prerequisites for optimal efficiency. The selected Tx current in Fig. 13(c), derived from (16), achieves an induced voltage peaking at 12 V with Tx currents at (0.2 A, 0.2 A, 0.43 A), and the system can transfer energy with an efficiency of 81.9%. By adjusting the input voltage rather than maintaining a consistent current across each Tx, the system's power transfer efficiency witnesses a notable enhancement.

Theoretically, the *LCC*-S configuration can deliver a consistent voltage output, irrespective of the load, even with three *LCC* circuits on the Tx side. In subsequent tests, variation in the load resistance was introduced, and the system's input voltage was monitored. The variations in the voltage of the Rx coil and the overall system efficiency in relation to the resistance adjustments are presented in Fig. 14.

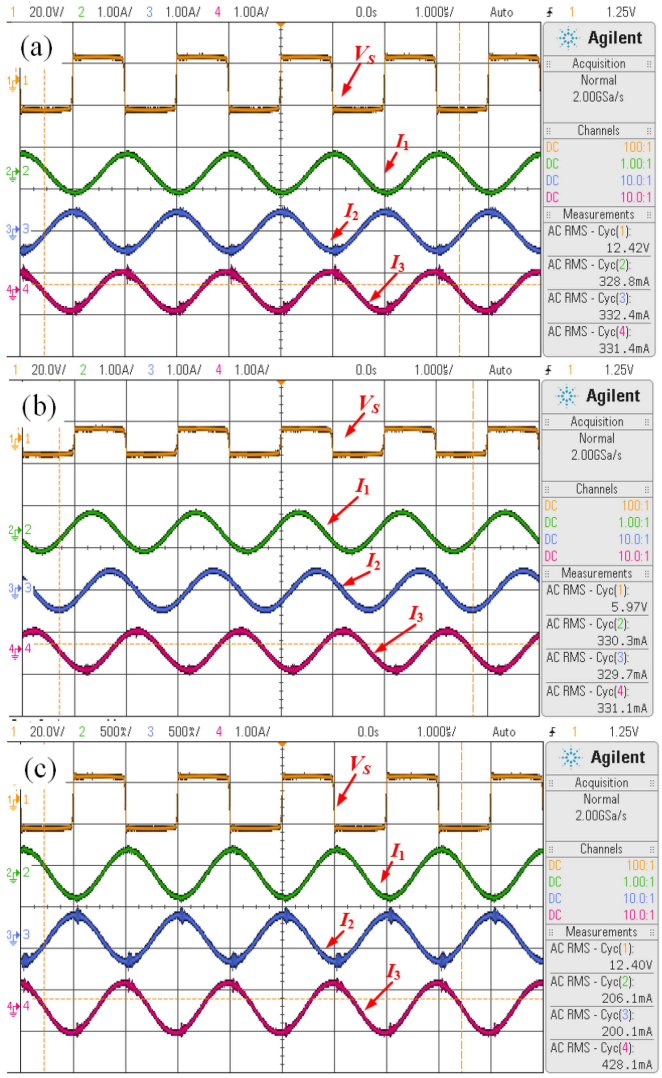

Fig. 13. Waveforms when (a) using the same Tx coil currents, (b) phases are 0, $\pi/6$, $\pi/3$, and (c) using the proposed method.

The results reveal that changes in resistance have a minimal effect on the output voltage across the Rx coil. As resistance increases, there is a slight elevation in the voltage at the Rx coil's terminals. This effect is likely due to the voltage division caused by the internal resistance within the receiving coil, which results in adjustments to the output voltage in response to variations in the load. Additionally, the efficiency of the system shifts in response to these load changes. Achieving optimal impedance matching, crucial for maximizing transfer efficiency, is possible when the load resistance is within the 20–30 Ω range. In such scenarios, the system is capable of attaining an efficiency peak of around 83%.

C. Position and Angular Misalignment

In WPT systems with high degrees of freedom, there is often an unpredictability regarding the receiver coil's placement. This necessitates a system capable of delivering power to the Rx with any specific location and orientation. To assess this, the

TABLE V
PERFORMANCE COMPARISONS OF SOME REPORTED OMNIDIRECTIONAL WPT SYSTEMS

Reported Works	Tx/Rx diameter	Number of inverters	Tx structure	Efficiency	Parameters needed for efficiency tracking
[12]	30/30 cm	3	Three orthogonal coils in 3-D space	About 28%	Rx's position information
[13]	50/10 cm	4	Planar coils	Up to 55%	No efficiency tracking
[14]	20/10 cm	More than 4	Planar coils	About 80%	Rx's position information
[21]	30/10 cm	3	Three orthogonal coils in 3-D space	About 11.5%	No efficiency tracking
[22]	58/10.5 mm	3	Three coils in one bowl area	Up to 28.5%	No efficiency tracking
[23]	6/4 cm	3	A Cube space with a side length of 6 cm	About 60%	No efficiency tracking
This article	10/3.5 cm	3	Planar coils	78%–83%	Primary side input currents

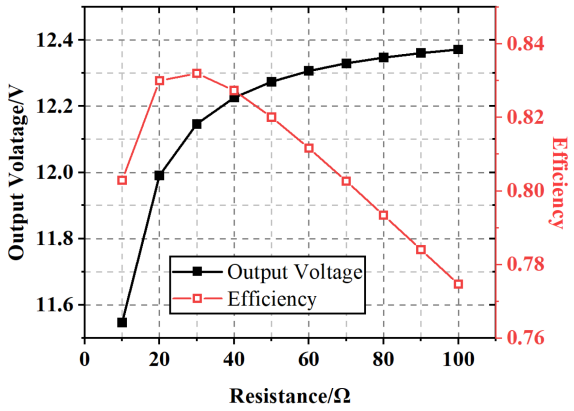

Fig. 14. Output voltage and efficiency during resistance changes.

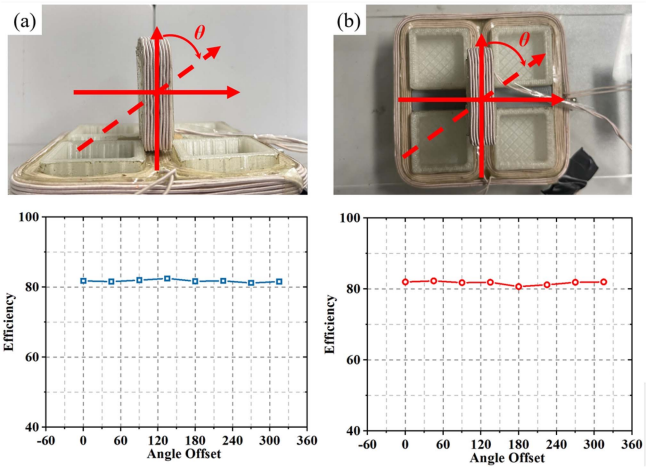

Fig. 15. Transfer efficiency during angular misalignments.

system's power transfer efficiency was examined with varied Rx alignments. Specifically, the Rx was located 2 cm directly above the Tx, with its plane's normal vectors at positions (1,0,0) and (1,1,0) in the experiments. Fig. 15 details the efficiency dynamics as the Rx underwent rotations about its horizontal axis.

Remarkably, regardless of the Rx's direction, the system consistently achieved a dc–dc output efficiency exceeding 80%. This confirms that the planar design of the Tx enables versatile power transmission irrespective of the Rx's orientation.

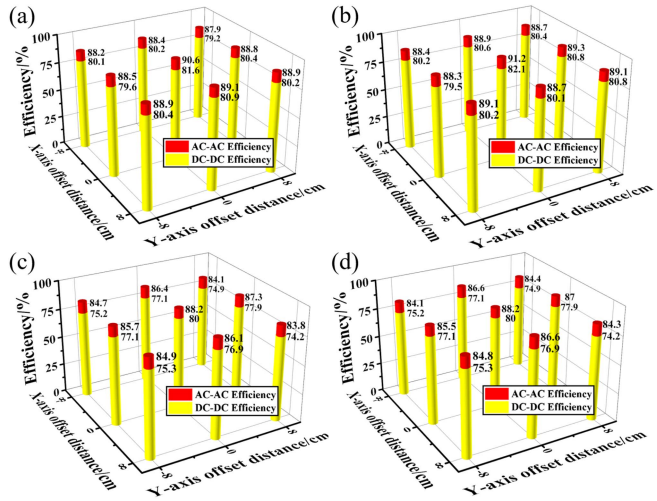

Fig. 16. Efficiency when the normal vectors of the Rx plane are (a) $(\sqrt{3}, 1, 1)$, (b) $(1, 1, \sqrt{3})$, (c) $(1, \sqrt{3}, 0)$, and (d) $(\sqrt{3}, 1, 0)$.

Further assessment is required for the power transfer capability when the Rx undergoes positional displacement. Experiments were executed with the Rx situated at various locations, specifically 2 cm above the Tx. And the normal vectors of the Rx plane are $(\sqrt{3}, 1, 1)$, $(1, 1, \sqrt{3})$, $(1, \sqrt{3}, 0)$, and $(\sqrt{3}, 1, 0)$, respectively. Fig. 11 visually represents the correlation between the Rx's placement and the achieved power transfer efficiency.

Fig. 16 demonstrates that the system maintains consistent efficiency regardless of the Rx's position. Moreover, the dc–dc efficiency exceeds 80% in the majority of areas, and sustained an ac efficiency of approximately 90%. Such a performance is unparalleled by conventional methods. Consequently, the introduced WPT system presents stable and high-efficiency solutions for devices demanding extensive spatial flexibility.

To achieve a more nuanced comprehension of the charging domain in the high-freedom WPT system, efficiency variations were assessed in relation to changes in the gap between the Rx center and the Tx plane. The normal vector of the Rx plane was designated as (1,0,0) (0,1,1), respectively. Fig. 17 portrays the efficiency fluctuations under these two orientations.

Clearly, the system experiences a significant drop in efficiency when the distance exceeds 4cm. This decrease is largely due to the reduced diameter of the Rx coil, which causes a significant decrease in mutual inductance as the distance grows. Changes in the orientation of the Rx result in only slight variations in

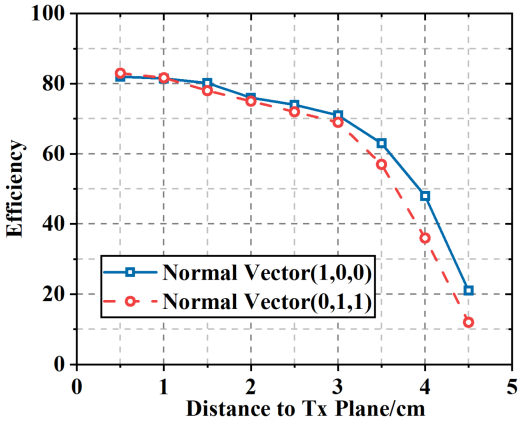

Fig. 17. Transfer efficiency with varying distance to Tx plane.

efficiency, a consequence of the distinct magnetic flux patterns created by the three Tx coils along the *Z*-axis. In conclusion, although this WPT system maintains steady efficiency across various angles and positions, achieving optimal performance necessitates proximity to the Tx. Table V provides a comparative analysis of performance metrics for various high degrees of freedom WPT systems from different studies, all of which utilize more than three inverters. Compared to some previous research, this article achieves efficient wireless energy transmission with stable efficiency, regardless of the position and orientation of the Rx coil. Furthermore, the approach introduced here is characterized by its simplicity and minimal parameter requirements, making it more straightforward to implement. Notably, the design utilizes an Rx coil that is comparatively smaller than the Tx coil, aligning more closely with the practical demands for wireless charging in devices requiring high mobility and flexibility.

VI. Conclusion

This article examines the transfer of power to a receiver in any position and orientation using a planar coil configuration. The underlying principles and design methodology for magnetic field shaping within the configuration are discussed. Subsequently, the CMT equations for the system were established. The theoretical analysis, simulations, and experimental results of this study indicate that there is a direct relationship between the dc input voltages and the currents of the inverters in achieving maximum efficiency. By altering the input voltages based on the measurement of currents in the inverters, it is possible to achieve magnetic field formation, thereby minimizing magnetic leakage and enhancing system efficiency. The method proposed in this article significantly enhances the efficiency of WPT systems that require high degrees of coupling freedom and compact configurations, such as in scenarios including mobile device charging and power provisioning for sensor networks.

References

[1] M. Wu et al., "Modeling of litz-wire DD coil with ferrite core for wireless power transfer system," *IEEE Trans. Power Electron.*, vol. 38, no. 5, pp. 6653–6669, May 2023.

[2] Y. Jiang, L. Wang, Y. Wang, J. Liu, X. Li, and G. Ning, "Analysis, design, and implementation of accurate ZVS angle control for EV's battery charging in wireless high-power transfer," *IEEE Trans. Ind. Electron.*, vol. 66, no. 5, pp. 4075–4085, May 2019.

[3] Y. Wu, H. Yuan, R. Zhang, A. Yang, X. Wang, and M. Rong, "Low-frequency wireless power transfer via rotating permanent magnets," *IEEE Trans. Ind. Electron.*, vol. 69, no. 10, pp. 10656–10665, Oct. 2022.

[4] X. Zhang et al., "A novel hybrid shielding method with single-source active topology and efficiency stability for wireless power transfer," *IEEE Trans. Magn.*, vol. 59, no. 11, Nov. 2023, Art. no. 8601006.

[5] H. Yuan et al., "A novel anti-offset interdigital electrode capacitive coupler for mobile desktop charging," *IEEE Trans. Power Electron.*, vol. 38, no. 3, pp. 4140–4151, Mar. 2023.

[6] C. Liang et al., "An anti-offset CPT system with multiple pickups for mobile desktop application," *IEEE Trans. Power Electron.*, vol. 39, no. 3, pp. 3826–3841, Mar. 2024.

[7] Y. Wu et al., "A universal coil structure design method with accurate numerical computation in wireless power transfer systems," in *Proc. IEEE Energy Convers. Congr. Expo.*, Nashville, TN, USA, 2023, pp. 6497–6504.

[8] S. Kim and B. Lee, "Control of magnetic field distribution by excitation phases of transmitters in MIMO WPT system," in *Proc. URSI Asia–Pac. Radio Sci. Conf.*, Seoul, South Korea, 2016, pp. 861–863, doi: 10.1109/URSIAP-RASC.2016.7601280.

[9] J. Song, M. Liu, and C. Ma, "Efficiency optimization and power distribution design of a megahertz multi-receiver wireless power transfer system," in *Proc. IEEE PELS Workshop Emerg. Technol., Wireless Power Transfer*, Chongqing, China, 2017, pp. 54–58.

[10] C. Zhang, D. Lin, and S. Y. Hui, "Basic control principles of omnidirectional wireless power transfer," *IEEE Trans. Power Electron.*, vol. 31, no. 7, pp. 5215–5227, Jul. 2016.

[11] Y. Lim and J. Park, "A novel phase-control-based energy beamforming techniques in nonradiative wireless power transfer," *IEEE Trans. Power Electron.*, vol. 30, no. 11, pp. 6274–6287, Nov. 2015.

[12] Q. Zhu, M. Su, Y. Sun, W. Tang, and A. P. Hu, "Field orientation based on current amplitude and phase angle control for wireless power transfer," *IEEE Trans. Ind. Electron.*, vol. 65, no. 6, pp. 4758–4770, Jun. 2018.

[13] N. Kang, Y. Shao, M. Liu, and C. Ma, "Analysis and implementation of 3D magnetic field shaping via a 2D planar transmitting coil array," *IEEE Trans. Power Electron.*, vol. 37, no. 1, pp. 1172–1184, Jan. 2022.

[14] T. Feng, Z. Zuo, Y. Sun, X. Dai, X. Wu, and L. Zhu, "A reticulated planar transmitter using a three-dimensional rotating magnetic field for free-positioning omnidirectional wireless power transfer," *IEEE Trans. Power Electron.*, vol. 37, no. 8, pp. 9999–10015, Aug. 2022.

[15] Z. Zhu et al., "Efficiency optimization and power allocation of omnidirectional wireless power transfer for multiple receivers," *IEEE Trans. Ind. Electron.*, vol. 70, no. 10, pp. 9689–9699, Oct. 2023.

[16] D. J. Griffiths, *Introduction to Electrodynamics*, 4th ed., New Int. Ed. London, U.K.: Pearson Educ., 2013, pp. 225–230.

[17] A. Kurs, A. Karalis, R. Moffatt, J. D. Joannopoulos, P. Fisher, and M. Soljačić, "Wireless power transfer via strongly coupled magnetic resonances," *Science*, vol. 317, no. 5834, pp. 83–86, Jul. 2007, doi: 10.1126/science.1143254.

[18] J. Wu, K. Li, J. Zeng, and S.-Y. R. Hui, "On the limitations of the coupled mode theory and parity-time symmetry for near-field wireless power transfer research," *IEEE Trans. Power Electron.*, vol. 39, no. 5, pp. 6433–6441, May 2024.

[19] C. Cheng, W. Li, Z. Zhou, Z. Deng, and C. Mi, "A load-independent wireless power transfer system with multiple constant voltage outputs," *IEEE Trans. Power Electron.*, vol. 35, no. 4, pp. 3328–3331, Apr. 2020.

[20] X. Wang, J. Xu, H. Ma, and P. Yang, "A high efficiency LCC-S compensated WPT system with dual decoupled receive coils and cascaded PWM regulator," *IEEE Trans. Circuits Syst. II, Express Briefs*, vol. 67, no. 12, pp. 3142–3146, Dec. 2020.

[21] H. Han, Z. Mao, Q. Zhu, M. Su, and A. P. Hu, "A 3D wireless charging cylinder with stable rotating magnetic field for multi-load application," *IEEE Access*, vol. 7, pp. 35981–35997, 2019.

[22] J. Kim, D.-H. Kim, J. Choi, K.-H. Kim, and Y.-J. Park, "Free-positioning wireless charging system for small electronic devices using a bowl-shaped transmitting coil," *IEEE Trans. Microw. Theory Techn.*, vol. 63, no. 3, pp. 791–800, Mar. 2015.

[23] H. Le-Huu and C. Seo, "Dual-band free-positioning transmitting coil for multiple-receiver wireless power transfer," *IEEE Access*, vol. 9, pp. 107298–107308, 2021.

Zhenghao Zhu received the B.S. degree in electrical engineering in 2018 from Xi'an Jiaotong University, Shaanxi, China, where he is currently working toward the Ph.D. degree in electrical engineering.

His research interests include wireless power transfer and power electronics.

Huan Yuan received the B.S. degree in electrical engineering from Southwest Jiaotong University, Chengdu, China, in 2014, and the Ph.D. degree in electrical engineering from the Department of Electrical Engineering, Xi'an Jiaotong University, Xi'an, China, in 2019.

He is currently an Assistant Professor with Xi'an Jiaotong University. His research interests include intelligent perception and system in complex electromagnetic environment, wireless power transfer, and artificial intelligence.

Cang Liang received the B.S. degree in electrical engineering from Southwest Jiaotong University, Chengdu, China, in 2019. He is currently working toward the Ph.D. degree in electrical engineering with the Department of Electrical Engineering, Xi'an Jiaotong University, Xi'an, China.

His current research focuses on wireless power transfer.

Chaoting Wang received the B.S. degree in electrical engineering from Chongqing University, Chongqing, China, in 2018. He is currently working toward the M.S. degree in electrical engineering with the Department of Electrical Engineering, Xi'an Jiaotong University, Xi'an, China.

His research interests include online monitoring and fault diagnosis of power equipment.

Simeng Lv was born in China, in 2000. She received the B.S. degree in electrical engineering from North China Electric Power University, Beijing, China, in 2022. She is currently working toward the master's degree in electrical engineering with the Department of Electrical Engineering, Xi'an Jiaotong University, Xi'an, China.

Her current research focuses on fault diagnosis of power equipment.

Aijun Yang (Senior Member, IEEE) received the B.S. and Ph.D. degrees in electrical engineering from the Department of Electrical Engineering, Xi'an Jiaotong University, Xi'an, China, in 2009 and 2014, respectively.

He is currently an Associate Professor with Xi'an Jiaotong University. His research interests include gas sensing based on nanomaterials, energy harvesters, and fault diagnosis.

Jifeng Chu (Member, IEEE) received the B.S. degree in electrical engineering from Southwest Jiaotong University, Chengdu, China, in 2016, and the Ph.D. degree in electrical engineering from the College of Electrical Engineering, Xi'an Jiaotong University, Xi'an, China, in 2021.

He is currently a Postdoctoral Researcher with Xi'an Jiaotong University. His research interests include the application of gas sensors and artificial intelligence technology in power equipment.

Mingzhe Rong (Senior Member, IEEE) received the B.S. and Ph.D. degrees in electrical engineering from Xi'an Jiaotong University, Xi'an, China, in 1984 and 1990, respectively.

He is currently a Professor with Xi'an Jiaotong University. His current research focuses on the detection and diagnosis techniques for electrical equipment and online monitoring technique.

Dr. Rong is an IET Fellow.

Xiaohua Wang (Senior Member, IEEE) received the B.S. degree in electrical engineering from Chang'an University, Xi'an, China, in 2000, and the Ph.D. degree in electrical engineering from the Department of Electrical Engineering, Xi'an Jiaotong University, Xi'an, China, in 2006.

He is currently a Professor with Xi'an Jiaotong University. His research interests include condition monitoring technique and fault diagnosis for electrical apparatus.

Aiguo Patrick Hu (Senior Member, IEEE) received the B.E. and M.E. degrees in electrical engineering from Xi'an Jiaotong University, Xi'an, China, in 1985 and 1988, respectively, and the Ph.D. degree in electrical engineering from the University of Auckland, Auckland, New Zealand, in 2001.

He was with the National University of Singapore for a semester as an exchange Postdoc Research Fellow. He is currently a Full Professor with the Department of Electrical and Electronic Engineering, University of Auckland. He has authored or coauthored more than 200 peer reviewed journal and conference papers with about 4500 citations, authored the first monograph on inductive power transfer technology, and contributed four book chapters on wireless power transfer modeling and control, as well as electrical machines. His research interests include wireless/contactless power transfer systems and application of power electronics in renewable energy systems.

Dr. Hu was the recipient of the University of Auckland VC's Funded Research and Commercialization Medal in April 2017.